Carbon Dioxide and Methane Fluxes at the Air-Sea Interface of Red Sea Mangroves

Mallory A. Sea[1], Neus Garcias-Bonet[1], Vincent Saderne[1]* and Carlos M. Duarte[1]

[1] {King Abdullah University of Science and Technology (KAUST), Red Sea Research Center (RSRC), Thuwal, 23955-6900, Saudi Arabia}

***Correspondence to: V. Saderne (vincent.saderne@kaust.edu.sa)**

Abstract

Mangrove forests are highly productive tropical and subtropical coastal systems that provide a variety of ecosystem services, including the sequestration of carbon. While mangroves are reported to be the most intense carbon sinks among all forests, they can also support large emissions of greenhouse gases (GHG), such as carbon dioxide (CO_2) and methane (CH_4), to the atmosphere. However, data derived from arid mangrove systems like the Red Sea are lacking. Here, we report net emission rates of CO_2 and CH_4 from mangroves along the eastern coast of the Red Sea, and assess the relative role of these two gases in supporting total GHG emissions to the atmosphere. Diel CO_2 and CH_4 emission rates ranged from -3452 to 7500 μmol CO_2 m^{-2} d^{-1} and from 0.9 to 13.3 μmol CH_4 m^{-2} d^{-1}, respectively. The rates reported here fall within previously reported ranges for both CO_2 and CH_4, but maximum CO_2 and CH_4 flux rates in the Red Sea are 10 to 100-fold below those previously reported for mangroves elsewhere. Based on the isotopic composition of the CO_2 and CH_4 produced, we identified potential origins of the organic matter that support GHG emissions. In all but one mangrove stand, GHG emissions appear to be supported by organic matter from mixed sources, potentially reducing CO_2 fluxes and instead enhancing CH_4 production, a finding that highlights the importance of determining the origin of organic matter in GHG emissions. Methane was the main source of CO_2-equivalents despite the comparatively low emission rates in most of the sampled mangroves, and therefore

deserves careful monitoring in this region. By further resolving GHG fluxes in arid mangroves, we will better ascertain the role of these forests in global carbon budgets.

1 Introduction

Mangrove forests, typically growing in the intertidal zones of tropical and subtropical coasts, are highly productive components of coastal ecosystems and adapted to high salinity and anoxic conditions associated with waterlogged sediments. Mangrove forests cover a global estimated area of 137,760 km^2 (Giri et al., 2011) and are typically constrained by temperature, with greatest biomass and species diversity in the equatorial zone (Alongi, 2012). Mangroves rank amongst the most threatened ecosystems in the biosphere, with losses estimated at 50% of their global extent over the past 50 years (Alongi, 2012). These losses affect nearly all mangrove regions but the Red Sea, where mangrove coverage has increased by 12% over the past four decades (Almahasheer et al., 2016).

Loss of mangrove forest represents a loss of valuable ecosystem services, including habitat and nursery for marine species, coastal protection from erosion due to wave action, and the filtration of harmful pollutants from terrestrial sources (Alongi, 2008), as well as loss of CO_2 sink capacity. Additionally, mangroves can become a source of greenhouse gas (GHG) emissions from disturbed soil carbon stocks (Donato et al., 2011; Alongi, 2014). Hence, mangrove conservation and restoration have been proposed as important components of so-called Blue Carbon strategies to mitigate climate change (Duarte, et al., 2013). Indeed, mangroves are reported to be the most intense carbon sinks among all forests, supporting carbon sequestration rates and organic carbon stocks as much as five times higher than those in terrestrial forests (Donato et al., 2011). While mangrove forests cover less than 1% of total coastal ocean area, they contribute to almost 15% of total carbon sequestration in coastal ecosystems (Alongi, 2012), making mangrove forests highly effective in terms of carbon sequestration per unit area. The management of mangroves to maximize CO_2 removal and subsequent storage is gaining momentum as a cost-effective strategy to mitigate climate change.

However, mangrove forests act as both carbon sinks and sources and have been reported to support large GHG emissions in the forms of CO_2 and CH_4 (Allen et al., 2007; Kristensen et al., 2008a; Chen et al., 2016). Whereas concerns are focused on GHG emissions following mangrove disturbance, estimated at 0.02 – 0.12 Pg C yr^{-1} globally (Donato et al., 2011), undisturbed

mangrove sediments also support GHG emissions (Purvaja and Ramesh, 2000; Kristensen et al., 2008b; Chauhan et al., 2015). Recent reports specifically highlight the importance of methane in flux estimates, as emissions of CH_4, with a higher global warming potential, can offset mangrove carbon burial by as much as 20% (Rosentreter et al., 2018b). Previous studies on GHG emission rates either focus on the soil-atmosphere interface, highlighting substantial flux ranges with mangroves reported to act as negligible (Alongi, 2005) to considerable sources (Livesley and Andrusiak, 2012; Chen et al., 2016), or examine net fluxes at the air-sea interface, with few studies in arid systems. Comparisons of carbon sequestration rates between mangrove stands have revealed that climatic conditions play an important role, with mangroves in the arid tropics, such as those in the Red Sea, supporting the lowest carbon sequestration rates (Almahasheer et al. 2017). Likewise, GHG emissions from mangrove forests may vary with climate, with most reported rates to-date derived from the wet tropics (Alongi et al., 2005; Chauhan et al., 2015; Chen et al., 2016). Whereas Red Sea mangroves are considered to play a minor role as CO_2 sinks, their role may be greater than portrayed by low carbon burial rates if they also support very low GHG emissions, thereby leading to a balance comparable to mangroves in the wet tropics.

Here we report air-sea emission rates of CO_2 and CH_4, along with their carbon isotopic composition, from incubations of inundated mangrove sediments cores along the Saudi coast of the Red Sea. We assess the relative role of these two gases in supporting total GHG emissions as well as their fluctuations along the day-night cycle.

2 Materials and Methods

2.1 Study area

We sampled seven mangrove forests along the eastern coast of the Red Sea (Fig. 1). We collected triplicate sediment cores by inserting translucent PVC tubes (30.5 cm in height and 9.5 cm in diameter) into mangrove sediments, collecting approx. 20 cm of sediment and a top seawater layer. The overlying water was regularly replaced by fresh seawater from the corresponding station in order to fill the remaining core volume and to measure CO_2 and CH_4 fluxes from underlying sediments during incubations. Mangrove sediments were sampled five to

ten meters from the forest edge, typically in the center of the mangrove belt. We sampled two stations (S1 and S2) in January and February 2017 and the other five mangrove stations (S3-S7) in March on board the R/V Thuwal as part of a scientific cruise. The cores collected from S1 and S2 were immediately transported to the laboratory, placed in seawater baths and enclosed in environmental growth chambers (Percival Scientific Inc., Perry, IA, USA) with 12:12 light cycles at a constant temperature of 26°C. The sediment cores collected during the scientific cruise were transported immediately on board and placed in open aquarium tanks with running seawater in order to keep them close to *in situ* temperature. Salinity and temperature were routinely recorded using a CTD. Additionally, sediment chlorophyll *a* and nutrient (organic carbon and nitrogen) content were analyzed from cores collected during the scientific cruise.

2.2 Sediment characteristics

The chlorophyll *a* content of the sediment was measured by fluorometry. The surface layer of each replicate core was collected and frozen until further analysis. Prior to chlorophyll *a* extraction, the sediment samples were left at room temperature to thaw. The chlorophyll *a* was extracted by adding 7 ml of 90% acetone to 2 ml of sediment sample. After a 24h incubation at 4^{o} C in dark conditions, the samples were centrifuged and the chlorophyll *a* content in the supernatant was measured on a Trilogy fluorometer. The nutrient (organic carbon and nitrogen) content of the sediment was analyzed on an Organic Elemental Analyzer (Flash 2000) after acidification of sediment samples.

2.3 Measurement of greenhouse gas fluxes

We measured CO_2 and CH_4 air-sea fluxes using two different techniques. The CO_2 and CH_4 fluxes from stations S1 and S2 were measured using the closed water circuit technique and the CO_2 and CH_4 fluxes from the rest of the stations sampled during the scientific cruise (S3-S7) were measured using the headspace technique.

2.3.1 Measurement of CO_2 and CH_4 fluxes in sediment core incubations using closed water circuit technique

We incubated mangrove sediment cores from stations S1 and S2 using a closed water circuit technique in order to measure changes in CO_2 and CH_4 concentrations. Before starting the incubation, the seawater above the sediment from each core was replaced by fresh seawater collected from the same location, avoiding disturbance of the sediment. Then, the seawater from the core was recirculated by a peristaltic pump in an enclosed water circuit through a membrane equilibrator (Liqui-cel mini module, 3M, Minnesota, USA). This setup enables the equilibration of gases in dissolution with an enclosed air circuit. The air from the enclosed air circuit was then passed through a desiccant column (calcium sulfate, WA Hammond Drierite Co., LTD, Ohio, USA) and flowed into a cavity ring-down spectrometer (CRDS; Picarro Inc., Santa Clara, CA, USA) to continuously measure the CO_2 and CH_4 concentration. We ran the incubations for at least 30 minutes under light (200 µmol photons m^{-2} s^{-1}) and dark conditions.

The concentration of CO_2 in the water circuit (µmol ml^{-1}) was calculated by Eq. (1):

$$[CO_2] = Hcp \times [HP\_CO_2] \times (1 - pH_20), \quad (1)$$

where Hcp is the Henry constant (mol ml^{-1} atm^{-1}) calculated using R marelac package (Soetaert et al., 2016); $[HP\_CO_2]$ is the given concentration of CO_2 (ppm), and pH_20 is the water vapor pressure (atm).

The CO_2 fluxes were calculated from the change in CO_2 concentration over time during our incubations, correcting by the seawater volume present in each core. Then, the fluxes were transformed to an aerial basis (µmol m^{-2} h^{-1}) by taking into account the core surface area. Finally, the daily fluxes (µmol m^{-2} d^{-1}) were calculated by multiplying the CO_2 flux obtained under light conditions by the number of light hours plus the CO_2 flux obtained under dark conditions by the number of dark hours.

The CH_4 fluxes were calculated in the same manner as for the CO_2 fluxes, with the exception that the Henry constant was calculated using Eq. (2):

$$\beta = Hcp \times (RT), \quad (2)$$

where Hcp is the Henry constant (mol ml^{-1} atm^{-1}), R is the ideal gas constant (82.057338 atm ml mol^{-1} K^{-1}), T is standard temperature (273.15 K), and β is the Bunsen solubility coefficient of CH_4, extracted from Wiesenburg and Guinasso (1979).

2.3.2 Measurement of CO_2 and CH_4 fluxes in sediment core incubations using the headspace technique

Mangrove sediment cores from stations S3 to S7 were incubated using a headspace technique in order to measure changes in CO_2 and CH_4 concentrations. Before starting the incubation, the seawater above the sediment from each core was replaced by fresh seawater from the running seawater system, leaving a headspace of 200 ml. Each core was sealed with a stopper equipped with a gas-tight valve serving as a headspace sampling port. The sealed core was left for 1 hour before the first headspace sampling to allow equilibration between seawater and air phases. Each core was sampled with a syringe, withdrawing 15 ml of air from the equilibrated headspace. Headspace samples were periodically drawn from each sediment incubation over a 24-hour incubation period. The CO_2 and CH_4 concentrations in the headspace samples along with their isotopic composition ($\delta^{13}C$-CO_2 and $\delta^{13}C$-CH_4) were measured with a CRDS (Picarro Inc., Santa Clara, CA, USA) connected to a small sample isotopic module extension (SSIM A0314, Picarro Inc., Santa Clara, CA, USA). We ran standards (730 ppm CO_2, 1.9 ppm CH_4) before and after every three samples.

The concentration of dissolved CO_2 in the seawater after equilibrium was calculated from the concentration in the equilibrated headspace (ppm) as described previously by Wilson et al. (2012) for other gases:

$$[CO_2]_w = 10^{-6} \beta \, m_a \, p_{dry}, \quad (3)$$

where β is the Bunsen solubility coefficient of CO_2 (mol ml^{-1} atm^{-1}), m_a is the given concentration of CO_2 in the equilibrated headspace (ppm), and p_{dry} is atmospheric pressure (atm) of dry air. The Bunsen solubility coefficient of CO_2 was calculated using Eq. (4):

$$\beta = \text{Hcp} \times (RT) \quad (4)$$

where Hcp is the Henry constant (mol ml^{-1} atm^{-1}) calculated using R marelac package (Soetaert et al., 2016), R is the ideal gas constant (82.057338 atm ml mol^{-1} K^{-1}) and T is standard temperature (273.15 K). The atmospheric pressure of dry air (p_{dry}) was calculated using Eq. (5):

$$p_{dry} = p_{wet} (1 - \%H_20) \quad (5)$$

where p_{wet} is the atmospheric pressure of wet air corrected by the effect of multiple syringe draws from the same core, applying Boyle's law.

The initial concentration of dissolved CO_2 in seawater before equilibrium was then calculated as:

$$[CO_2]_{aq} = ([CO_2]_w V_w + 10^{-6} m_a V_a) / V_w \quad (6)$$

where $[CO_2]_w$ is the concentration of dissolved CO_2 in the seawater after equilibrium, V_w is the volume of seawater (ml) and V_a is the headspace volume (ml) in the core. Finally, treating the gas as ideal, the units were converted to nM using Eq. (7):

$$[CO_2]_{aq} = 10^9 * p_{dry}[CO_2]_{aq} / (RT) \quad (7)$$

where R is the ideal gas constant (0.08206 atm l mol^{-1} K^{-1}) and T is temperature (K).

The CO_2 fluxes were calculated from the change in CO_2 concentration over time during our incubations, correcting by the seawater volume present in each core. Then, the fluxes were transformed to an aerial basis (µmol m^{-2} d^{-1}) by taking into account the core surface area. Finally, the day and night fluxes (µmol m^{-2} h^{-1}) were calculated from the change in CO_2 concentration between consecutive samplings during day and night time, respectively.

The CH_4 fluxes were calculated in the same manner as for the CO_2 fluxes, with the exception that the Bunsen solubility coefficient of CH_4 was calculated according to Wiesenburg and Guinasso (1979).

2.4 Isotopic composition of CO_2 ($\delta^{13}C$- CO_2) and CH_4 ($\delta^{13}C$- CH_4)

The isotopic signature of the CO_2 and CH_4 produced during incubations was estimated by conducting keeling plots (Pataki et al. 2003; Thom et la. 2003; Garcias-Bonet and Duarte 2017). Briefly, the $\delta^{13}C$ of the CO_2 and CH_4 produced was extracted from the intercept of the linear regression between the inverse of the gas partial pressure and the isotopic signature.

The data set is available from Sea et al. (2018).

3 Results

The mean (± SE) diel CO_2 and CH_4 emission rates for the seven sites were 372 ± 1309 µmol CO_2 m^{-2} d^{-1} and 5.6 ± 1.6 µmol CH_4 m^{-2} d^{-1}, respectively. We observed high variability among the seven mangrove forest sites studied, with net CO_2 and CH_4 diel emission rates ranging from -3452 to 7500 µmol CO_2 m^{-2} d^{-1} and from 0.9 to 13.3 µmol CH_4 m^{-2} d^{-1}, respectively (Table 1).

Mangrove sediments absorbed CO_2 during daytime and emitted CO_2 during night time at 5 out of 7 stations, with means (± SE) of -54.6 ± 37 µmol CO_2 m^{-2} h^{-1} and 86 ± 120 µmol CO_2 m^{-2} h^{-1} respectively (Table 1, Fig. 2). However, in three out of seven sites, heterotrophic activities outbalanced photosynthesis on a 24h basis. At two sites, S3 and S6, we found an increase of the CO_2 emissions between day and night, contradictory to the classical daytime primary production–night-time respiration pattern, possibly indicative of a light mediated increase of heterotrophic processes.

Methane emissions did not show circadian patterns with linear increases in CH_4 concentration in our incubations (Fig. 2) and with similar light and dark rates (0.26 ± 0.08 and 0.21 ± 0.07 µmol CH_4 m^{-2} h^{-1} (mean ± SE), respectively (Table 1). In terms of total GHG contribution, the mean CO_2-equivalents (CO_2e) emission to the atmosphere was 564 ± 1284 µmol CO_2e m^{-2} d^{-1} (mean ± SE) using the 100 years' time horizon global warming potential (Myhre et al., 2013). Inundated mangrove sediments were net emitters of CO_2e in three out of seven sites (Table 1), and in five out of seven mangrove stands sampled, CH_4 was the main source of CO_2e to the atmosphere.

While no overall trend was revealed through the relationship between day and night fluxes for CO_2 and CH_4 (Fig. 3), consistencies are evident at specific mangrove stations. For example, night CO_2 emissions are clearly visible at S2, while S3 appears to emit CO_2 during daylight hours. No relationship was apparent between GHG fluxes and the densities of organic carbon or nitrogen in the sediment. There was no discernible trend between gas fluxes and chlorophyll *a* content in surface sediments.

The isotopic signatures of the produced CO_2 ($\delta^{13}C$-CO_2) ranged from -11.21 to -25.72 ‰ as derived from keeling plots (Fig. 4, Table 1). The $\delta^{13}C$-CO_2 was similar for almost all stations, with the exception of S3 that had a $\delta^{13}C$-CO_2 of -25.72 ‰. The isotopic composition of the produced CH_4 ($\delta^{13}C$-CH_4) ranged from -71.28 to -87.08 ‰, with a mean $\delta^{13}C$ signature of -80.61 ‰ (Fig. 4, Table 1).

4 Discussion

4.1 Greenhouse gas fluxes

The CO_2 and CH_4 emissions reported in this study show that Red Sea mangroves can act as a source of GHG to the atmosphere. Values reported from this study fall within previously reported ranges for both CH_4 and CO_2, but maximum CH_4 and CO_2 flux rates in the Red Sea are up to 100 fold below those reported elsewhere. Compiled global values for GHG fluxes range from -16.9 to 629.2 mmol CO_2 m^{-2} d^{-1} and -2.1 to 25,974 µmol CH_4 m^{-2} d^{-1}, with mean (±SE) maximum emission rates averaging 202.3 ± 48 mmol m^{-2} d^{-1} and 4783.6 ± 2783 µmol m^{-2} d^{-1} for CO_2 and CH_4 respectively (Table 2).

The variability in GHG emission rates reported in this study could be attributed to spatial differences, as cores were taken from different parts of each forest. Indeed, previous studies report significant discrepancies in emission rates in fringe versus forest positions (Allen et al., 2007). Additionally it is possible that differences in flux rates may exist as a result of sediment disturbance from the coring process. The effects of mangrove pneumatophores and possible bioturbation from infaunal species such as burrowing crabs were not considered here yet could

pose another possible source of variation in results as the presence of these structures influences oxygenation of sediment and pore water exchange, identified as driving factors in varying CO_2 levels (Call et al., 2014; Rosentreter et al., 2018). These factors likely affect relevant redox processes and would therefore be useful to quantify in future studies.

Uniformity of day and night emission rates for CH_4 was observed in Red Sea mangrove stands, with mean (± SE) CH_4 emission rates of 0.28 ± 0.08 µmol CH_4 m^{-2} h^{-1} during the day and 0.24 ± 0.08 µmol CH_4 m^{-2} h^{-1} during night; this is consistent with previous work reporting that emission rates for CH_4 do not vary significantly during light and dark hours in mangrove forests (Allen et al., 2007). It has been suggested instead that variables such as sediment temperature are more significant in their contributions to emission rates (Allen et al., 2007; Allen et al., 2011). Incubated sediment cores kept at constant temperature do not reflect the range of temperatures experienced by mangrove sediments over the diurnal cycle; future studies examining GHG emissions under more realistic temperature fluctuations are needed. Seasonal studies of longer duration have reported increased emission rates during warmer seasons (Chen et al., 2016; Livesley and Andrusiak, 2012). Methane concentrations typically remain low due to anaerobic methane oxidation processes that take place near sediment surfaces (Kristensen et al., 2008a), consistent with the low CH_4 emission rates from Red Sea mangrove sediments observed here. Additionally, environments of high salinity like the Red Sea have been associated with decreased CH_4 emissions, as sulfate-reducing bacteria are thought to outcompete methanogens (Poffenbarger et al., 2011).

Methane emission rates at the air-sea interface of Red Sea mangrove sediments, although quite low, become more substantial when considered in terms of global warming potential. In this study, CH_4 was, despite the comparatively low emission rates, the main source of CO_2e in the majority of sampled mangroves, and therefore deserves careful monitoring in this region. Reported organic carbon burial rates of Red Sea mangroves of 3.42 mmol C m^{-2} d^{-1} (Almahasheer et al. 2017) are 10 times larger than the combined average CO_2 and CH_4 emission rates reported here (0.37 mmol C m^{-2} d^{-1}), suggesting that these mangrove sediments could act as net atmospheric carbon sinks; however, significant alkalinity and DIC exports have been identified from mangroves as well (Sippo et al., 2016), necessitating future studies which

297 measure these exports to neighboring habitats in order to close the carbon budget and determine
298 the role of Red Sea mangroves in potential climate change mitigation. Currently, protection
299 measures and further reforestation efforts are being deployed along the Red Sea that will further
300 expand the area of mangroves (Almhasheer et al. 2016). The rationale for conserving mangroves
301 in the climate change context is not adequately represented by their net carbon sink capacity
302 when undisturbed, but rather by the emissions resulting from their disturbance. Indeed, previous
303 studies analyzing anthropogenic impacts on methane emission rates from mangrove sediments
304 have shown that disturbance significantly increases methane emissions (Purvaja and Ramesh,
305 2001; Chen et al., 2011). This provides an additional rationale to conserve, and continue to
306 expand, Red Sea mangroves.
307
308 While this study provides new insights on GHG fluxes from arid mangroves, the methods used
309 here solely measure the air-sea fluxes of dissolved gases. If CO_2 is produced from underlying
310 sediments, it enters the water column and becomes a part of the carbonate system, with
311 possibility of conversion to bicarbonate (HCO_3^-) and carbonate (CO_3^{2-}) ions; these dominating
312 species represent over 99% of the dissolved inorganic carbon (DIC) under current atmospheric
313 and oceanic conditions (Zeebe and Wolf-Gladrow, 2001). Therefore, the air-sea equilibration
314 methods used in this study do not measure DIC fluxes, but only the fluxes of the dissolved CO_2-
315 component of this larger system.
316
317 Frankignoulle and Borges (2001) show that CO_2 can be measured either directly (using
318 equilibrator techniques and spectroscopy or chromatography) or indirectly (by making
319 calculations based on pH, total alkalinity, and DIC). The methodology presented in this study
320 represents the former, utilizing an air-sea equilibrator connected to a CRDS to measure GHG
321 fluxes at the air-sea interface. Research conducted by Borges et al. (2003) utilizes the indirect
322 approach, using pH and total alkalinity measurements in Papua New Guinea to calculate DIC
323 and $CO_{2(dis)}$ (for a computational discussion see Frankignoulle and Borges, 2001). Both methods
324 measure at the air-sea interface (Table Two) but are not directly comparable, as a full
325 determination of the carbonate system was not carried out in the present study. Similarly, studies
326 using equilibrator techniques that measure the dissolved CO_2 fraction of seawater to the
327 atmosphere are influenced by the seawater carbonate system and further steps of isotopic fraction

(discussed below), and are therefore not directly comparable to those studies which measure GHG fluxes from exposed mangrove sediments to the atmosphere (Table Two).

4.2 Isotopic composition of emitted gases

There were no relationships between GHG fluxes and sediment properties, such as chlorophyll *a*, nitrogen density, and organic carbon density, suggesting that other factors have greater influence on GHG flux rates in this region. Since mangroves can receive large contributions of organic carbon from other sources (Newell et al., 1995), such as algal mats, seagrass and seaweed, examination of the isotopic composition of emitted carbon provides insights into the origin of the organic carbon supporting GHG fluxes in mangrove sediments; however, it should be noted that $\delta^{13}C$ values reported in this study occur after several steps of isotopic fractionation and may therefore influence results. Isotope effects can cause an unequal distribution of isotopes between DIC components; for example as CO_2 is produced from mangrove sediments and becomes part of the carbonate system (likely forming HCO_3^- after equilibration), molecules containing the heavier carbon isotope—with a higher activation energy—will typically react more slowly (Zeebe and Wolf-Gladrow, 2001), promoting a higher concentration of the heavy isotope in unreacted CO_2 and a relative depletion of this heavier isotope in resulting HCO_3^-. Similarly, this preferential incorporation and movement of molecules containing lighter isotopes can affect resulting carbon isotope ratios after air-sea equilibration (with depletion of lighter isotopes in seawater as a result of fractionation). CO_2 measured in this study is subject to these processes and may not reflect the isotopic ratios of carbon originally emitted; rather, the signatures measured in this study should be seen as a proxy which reflects isotopic ratios of air-sea discrimination and biological processing (decomposition, respiration, and photosynthesis), resulting after carbon isotope fractionation. Interpretation of results is therefore subject to this limitation.

The isotopic signature of the CO_2 ($\delta^{13}C$-CO_2) produced by mangrove sediments in four out of the five mangrove stands with available isotopic data was heavier (from -11.2 ± 0.6 to -15.9 ± 1.1 ‰; Table 1) than the isotopic signature of mangrove tissues, suggesting decomposition of organic matter from mixed sources (Kennedy et al. 2010). Specifically, the isotopic signature of

359 the mangroves found in the central Red Sea has been recently reported as $\delta^{13}C_{leaves}$ = -26.98 ±
360 0.15 ‰, $\delta^{13}C_{stems}$ = -25.75 ± 0.16 ‰ and $\delta^{13}C_{roots}$ = -24.90 ± 0.17 ‰ for mangrove leaves, stems
361 and roots while the mean isotopic signature of other primary producers in the central the Red Sea
362 has been reported as $\delta^{13}C_{seaweed}$ = -12.8 ± 0.5 ‰ and $\delta^{13}C_{seagrass}$ = -8.2 ± 0.2 ‰ for seaweed and
363 seagrass tissues, respectively (Almahasheer et al. 2017). However, in one mangrove stand (S3)
364 the $\delta^{13}C$-CO_2 was much lighter (-25.72 ± 0.21 ‰), potentially indicating mangrove tissues. Thus,
365 according to the isotopic signature, the CO_2 produced in mangrove sediments would be
366 supported by mangrove biomass in only one mangrove stand out of the five sampled sites with
367 available isotopic data. Moreover, the mean isotopic signature of the CH_4 produced in mangrove
368 sediments ($\delta^{13}C$-CH_4 = -80.6 ‰) tentatively confirms its biogenic origin, which normally ranges
369 from -40 to -80 ‰, depending on the isotopic signature of the organic compounds being
370 biologically decomposed (Reeburgh, 2014). The lowest $\delta^{13}C$-CH_4 was detected in S3, coinciding
371 with the lowest $\delta^{13}C$-CO_2 value, suggesting that the organic matter being decomposed by
372 methanogens likely came from mangrove tissues as well.
373
374 Interestingly, the mangrove with the lightest $\delta^{13}C$-CO_2 and $\delta^{13}C$-CH_4 (S3), showed the lowest
375 daily CO_2 flux (-1524 ± 686 µmol CO_2 m^{-2} d^{-1}) but the highest CH_4 emission rate (13.3 ± 9.5
376 µmol CH_4 m^{-2} d^{-1}), compared to the fluxes detected in the rest of mangrove stands with available
377 isotopic data. Part of the variability in the CO_2 (R^2 = 0.42) and CH_4 (R^2 = 0.40) emission rate
378 seems to be explained by the origin of the organic matter being decomposed, estimated here as
379 the $\delta^{13}C$-CO_2 and $\delta^{13}C$-CH_4. Organic matter with lighter isotopic composition could enhance
380 CO_2 emissions, whereas organic matter with heavier isotopic composition could enhance CH_4
381 emissions (Fig. 5), possibly suggesting a different preferential use of organic matter by different
382 microbial groups in mangrove sediments. Future studies exploring this idea with further
383 considerations of carbon isotope fractionation would help solidify the role of the origin of
384 organic carbon stored in mangrove sediments on their GHG emissions.
385
386 **5 Conclusion**
387
388 This study is first in reporting CO_2 and CH_4 fluxes from Red Sea mangrove sediments,
389 contributing to the scant data on arid mangrove systems (Atwood et al. 2017, Almahasheer et al.

2017), essential to establish a solid baseline on GHG emissions for future studies. Results show that maximum CO_2 and CH_4 flux rates from Red Sea mangrove sediments are well below those reported elsewhere, and that, even when considered in terms of CO_2 equivalents, carbon burial rates largely outweigh GHG emission rates at the air-sea interface in this region. This study also highlights the importance of determining the source of organic matter in GHG flux studies, as emissions appear to be supported by organic matter from mixed sources in the majority of studied mangroves, potentially enhancing CH_4 production over CO_2 fluxes in this system. Seasonal variation should be considered in future studies on GHG emissions by Red Sea mangroves to better determine annual emission rates from this system, which reaches some of the warmest temperatures experienced by mangrove forests worldwide. Similarly, a wider spatial coverage within the mangrove forest should be considered to confidently determine net GHG fluxes that can be upscaled to the entire stock of Red Sea mangroves.

Methods presented in this study include the use of an air-sea equilibrator connected to a CRDS to measure GHG fluxes at the air-sea interface, measuring the dissolved CO_2-component of the larger seawater carbonate system. This methodology is one of many used to measure GHG flux rates; establishing a unified sampling technique at both the soil-atmosphere and air-seawater interface will aid future researchers in determining total carbon budgets and accurately informing policymakers of their findings. In combination with consideration of isotope effects, a full determination of the carbonate system will be beneficial in future studies to further resolve GHG fluxes in arid mangroves, allowing us to better ascertain the role of these forests in global carbon budgets.

Data availability. All data will be accessible in the repository Pangea pending manuscript acceptance.

Competing interests. The authors declare that they have no conflict of interest.

Author contribution

MAS, NG-B, VS and CMD designed the study. MAS and NG-B performed the measurements and calculations. MAS, NG-B, VS and CMD interpreted the results. All authors contributed substantially to the final manuscript.

Acknowledgements

This research was funded by King Abdullah University of Science and Technology (KAUST) through baseline funding to C.M.D. We thank D. Krause-Jensen, N. Massoudi, and K. Baldry for help during sampling, and the captain and crew of KAUST R/V Thuwal for support. M.A.S. was supported by King Abdullah University of Science and Technology through the VRSP program. We thank P. Carrillo de Albornoz for lab instrument support, and M. Ennasri for help with sediment analysis.

References

Allen, D. E., Dalal, R. C., Rennenberg, H., Meyer, R., L., Reeves, S., and Schmidt, S.: Spatial and temporal variation of nitrous oxide and methane flux between subtropical mangrove sediments and the atmosphere, Soil. Biol. Biochem., 39, 622-631, 2007.

Allen, D. E., Dalal, R.C., Rennenberg, H., and Schmidt, S.: Seasonal variation in nitrous oxide and methane emissions from subtropical estuary and coastal mangrove sediments, Australia, Plant. Biol., 13, 126-133, 2011.

Almahasheer, H., Aljowair, A., Duarte, C. M., and Irigoien, X.: Decadal stability of Red Sea mangroves, Estuar. Coast. Shelf. S., 169, 164-172, 2016.

Almahasheer, H., Serrano, O., Duarte, C. M., Arias-Ortiz, A., Masque, P., and Irigoien, X.: Low carbon sink capacity of Red Sea mangroves, Scientific Reports, 7, 9700, doi:10.1038/s41598-017-10424-9, 2017.

Alongi, D. M.: Mangrove forests: Resilience, protection from tsunamis, and responses to global climate change, Estuar. Coast. Shelf. S., 76, 1-13, 2008.

Alongi, D. M.: The energetics of mangrove forests, Springer Press, London, England, 2009.

Alongi, D. M.: Carbon sequestration in mangrove forests, Carbon. Manag., 3, 313-322, doi: 10.4155/cmt.12.20, 2012.

Alongi, D. M.: Carbon cycling and storage in mangrove forests, Annu. Rev. Mar. Sci., 6, 195-219, doi: 10.1146/annurev-marine-010213-135020, 2014.

Alongi, D. M., Pfitzner, J., Trott, L. A., Tirendi, F., Dixon, P., and Klumpp, D. W.: Rapid sediment accumulation and microbial mineralization in forests of the mangrove Kandelia candel in the Jiulongjiang Estuary, China, Estuar. Coast. Shelf. S., 63, 605-618, 2005.

462 Atwood, T. B., Connolly, R. M., Almahasheer, H., Carnell, P., Duarte, C. M., Ewers, C.,
463 Irigoien, X., Kelleway, J., Lavery, P. S., Macreadie, P. I., Serrano, O., Sanders, C., Santos, I.,
464 Steven, A., and Lovelock, C. E.: Global patterns in mangrove soil carbon stocks and losses, Nat.
465 Clim. Change, 7, 523-529, doi:10.1038/nclimate3326, 2017.
466
467 Borges, A. V., Djenidi, S., Lacroix, G., Theate, J., Delille, B., and Frankignoulle, M.:
468 Atmospheric CO_2 flux from mangrove surrounding waters, Geophys. Res. Lett., 30, 1558,
469 doi:10.1029/2003GL017143, 2003.
470
471 Bouillon, S., Frankignoulle, M., Dehairs, F., Velimirov, B., Eiler, A., Gwenael, A., Etcheber, H.,
472 and Borges, A. V.: Inorganic and organic carbon biogeochemistry in the Gautami Godavari
473 estuary (Andhra Pradesh, India) during pre-monsoon: The local impact of extensive mangrove
474 forests, Global. Biogeochem. Cy., 17, 1114, doi:10.1029/2002GB002026, 2003.
475
476 Bouillon, S., Dehairs, F., Schiettecatte, L., and Alberto Vieira Borges, A. V.: Biogeochemistry of
477 the Tana estuary and delta (northern Kenya), Limnol. Oceanogr., 52, 46-59, 2007a.
478
479 Bouillon, S., Dehairs, F., Velimirov, B., Gwenael, A., and Borges, A. V.: Dynamics of organic
480 and inorganic carbon across contiguous mangrove and seagrass systems (Gazi Bay, Kenya), J.
481 Geophys. Res., 112, G02018, doi:10.1029/2006JG000325, 2007b.
482
483 Bouillon, S., Middelburg, J. J., Dehairs, F., Borges, A. V., Abril, G., Flindt, M. R., Ulomi, S.,
484 and Kristensen, E.: Importance of intertidal sediment processes and porewater exchange on the
485 water column biogeochemistry in a pristine mangrove creek (Ras Dege, Tanzania),
486 Biogeosciences, 4, 317-348, 2007c.
487
488 Call, M., Maher, D. T., Santos, I. R., Ruiz-Halpern, S., Mangion, P., Sanders, C. J., Erler, D. V.,
489 Oakes, J. M., Rosentreter, J., Murray, R., and Eyre, B. D.: Spatial and temporal variability of
490 carbon dioxide and methane fluxes over semi-diurnal and spring-neap-spring timescales in a
491 mangrove creek, Geochimica et Cosmochimica Acta, 150, 211-225, 2015.

Chauhan, R., Datta, A., Ramanathan, A. L., and Adhya, T. K.: Factors influencing spatio-temporal variation of methane and nitrous oxide emission from a tropical mangrove of eastern coast of India, Atmos. Environ., 107, 95-106, 2015.

Chen, G., Tam, N. F. Y., Wong, Y. S., and Ye, Y.: Effect of wastewater discharge on greenhouse gas fluxes from mangrove soils, Atmos. Environ., 45, 1110-1115, 2011.

Chen, G., Chen, B., Yu, D., Tam, N. F. Y., Ye, Y., and Chen, S.: Soil greenhouse gas emissions reduce the contribution of mangrove plants to the atmospheric cooling effect, Environ. Res. Lett., 11,1-10, doi:10.1088/1748-9326/11/12/124019, 2016.

Duarte, C. M., Losada, I. J., Hendriks, I. E., Mazarrasa, I., and Marbà, N.: The role of coastal plant communities for climate change mitigation and adaptation, Nat. Clim. Change, 3, 961-968, doi: 10.1038/NCLIMATE1970, 2013.

Donato, D. C., Kauffman, J. B., Murdiyarso, D., Kurnianto, S., Stidham, M., and Kanninen, M.: Mangroves among the most carbon-rich forests in the tropics, Nat. Geosci., 4, 293-297, doi: 10.1038/NGEO1123, 2011.

Frankignoulle, M., and Borges, A. V.: Direct and indirect pCO_2 measurements in a wide range of pCO_2 and salinity values (the Scheldt Estuary), Aquat. Geochem., 7, 267-273, 2001.

Garcias-Bonet, N. and Duarte, C. M.: Methane production by seagrass ecosystems in the Red Sea, Frontiers in Marine Science, 4, 340, doi: 10.3389/fmars.2017.00340, 2017.

Giri, C., Ochieng, E., Tieszen, L. L., Zhu, Z., Singh, A., Loveland, T., Masek, J., and Duke, N.: Status and distribution of mangrove forests of the world using earth observation satellite data, Global. Ecol. Biogeogr., 20, 154-159, 2011.

Ho, D. T, Ferrón, S., Engel, V. C., Larsen, L. G., and Barr, J.G.: Air-water gas exchange and CO2 flux in a mangrove-dominated estuary, Geophys. Res. Lett., 41, 108-113, doi:10.1002/2013GL058785, 2014.

Jacotot, A., Marchand, C., and Allenbach, M.: Tidal variability of CO_2 and CH_4 emissions from the water column within a Rhizophora mangrove forest (New Caledonia), Sci. Total. Environ., 631, 334-340, 2018.

Kanninen, M.: Mangroves among the most carbon-rich forests in the tropics, Nat. Geosci., 4, 293-297, doi:10.1038/ngeo1123, 2011.

Kennedy, H., Beggins, J., Duarte, C. M., Fourqurean, J. W., Holmer, M., Marbà, N., and Middelburg, J. J.: Seagrass sediments as a global carbon sink: isotopic constraints, Global. Biogeochem. Cy., 24, GB4026, doi: 10.1029/2010GB003848, 2010.

Kristensen, E., Bouillon, S., Dittmar, T., and Marchand, C.: Organic carbon dynamics in mangrove ecosystems: A review, Aquat. Bot., 89, 201-219, doi:10.1016/j.aquabot.2007.12.005, 2008a.

Kristensen, E., Flindt, M. R., Ulomi, S., Borges, A. V., Abril, G., and Bouillon, S.: Emissions of CO_2 and CH_4 to the atmosphere by sediments and open waters in two Tanzanian mangrove forests, Mar. Ecol. Prog. Ser., 370, 53-67, doi: 10.3354/meps07642, 2008b.

Livesley, S. J., and Andrusiak, S. M.: Temperate mangrove and salt marsh sediments are a small methane and nitrous oxide source but important carbon store, Estuar. Coast. Shelf. Sci., 97, 19-27, 2012.

Myhre, G., Shindell, D., Bréon, F. M., Collins, W., Fuglestvedt, J., Huang, J., Koch, D., Lamarque, J. F., Lee, D., Mendoza, B., and Nakajima, T.: Anthropogenic and natural radiative forcing, Climate Change, 423, 2013.

Newell, R. I. E., Marshall, N., Sasekumar, A., and Chong, V. C.: Relative importance of benthic microalgae, phytoplankton, and mangroves as sources of nutrition for penaeid prawns and other coastal invertebrates from Malaysia, Mar. Biol., 123, 595-606, 1995.

554
555 Pataki, D., Ehleringer, J. R., Flanagan, L. B., Yakir, D., Bowling, D. R., Still, C. J., Buchmann,
556 N., Kaplan, J. O., and Berry, J. A.: The application and interpretation of Keeling plots in
557 terrestrial carbon cycle research, Global. Biogeochem. Cy., 17, 1022, doi:
558 10.1029/2001GB001850, 2013.
559
560 Poffenbarger, H. J., Needelman, B. A., and Megonigal, J. P.: Salinity influence on methane
561 emissions from tidal marshes, Wetlands, 31, 831-842, doi: 10.1007/s13157-011-0197-0, 2011.
562 Purvaja, R. and Ramesh, R.: Human impacts on methane emission from mangrove ecosystems in
563 India, Reg. Environ. Change., 1, 86-97, doi: 10.1007/PL00011537, 2000.
564
565 Purvaja, R. and Ramesh, R.: Natural and anthropogenic methane emission from wetlands of
566 south India, Environ. Manage., 27, 547-557, doi: 10.1007/s002670010169, 2001.
567 Reeburgh, W. S.: Global Methane Biogeochemistry Treatise on Geochemistry (Second Edition),
568 Holland, H. D., and Turekian, K. K., Oxford, Elsevier, 71-94, 2014.
569
570 Rosentreter, J. A., Maher, D. T., Erler, D. V., Murray, R., and Eyre, B. D.: Seasonal and
571 temporal CO_2 dynamics in three tropical mangrove creeks- A revision of global mangrove CO_2
572 emissions, Geochimica et Cosmochimica Acta, 222, 729-745, 2018a.
573
574 Rosentreter, J. A., Maher, D. T., Erler, D. V., Murray, R. H., and Eyre, B. D. Methane emissions
575 partially offset “blue carbon” burial in mangroves, Sci. Adv., 4, eaao4985, 2018b.
576
577 Sea, M. A., Garcias-Bonet, N., Saderne, V., and Duarte, C. M.: Data set on methane emissions
578 from Red Sea mangrove sediments. Pangea DOI: [data set will be published in the Pangea open
579 data repository at the acceptance of paper], 2018.
580
581 Sippo, J. Z., Maher, D. T., Tait, D. R., Holloway, C., and Santos, I. R.: Are mangroves drivers or
582 buffers of coastal acidification? Insights from alkalinity and dissolved inorganic carbon export
583 estimates across a latitudinal transect, Global. Biogeochem. Cy., 30: 753-766, 2016.

584 Soetaert, K., Petzoldt, T., and Meysman, F.: Marelac: A tool for aquatic sciences (R package),
585 available at: https://cran.r-project.org/web/packages/marelac/marelac.pdf, 2016.
586
587 Thom, M., Bosinger, R., Schmidt, M., and Levin, I.: The regional budget of atmospheric
588 methane of a highly populated area, Chemosphere, 26, 143-160, doi: 10.1016/0045-
589 6535(93)90418-5, 1993.
590
591 Wiesenburg, D. A. and Guinasso, N. L.: Equilibrium solubilities of methane, carbon monoxide,
592 and hydrogen in water and sea water, J. Chem. Eng. Data., 24, 356-360, 1979.
593
594 Wilson, S. T., Böttjer, D., Church, M. J., and Karla, D. M.: Comparative assessment of nitrogen
595 fixation methodologies, conducted in the oligotrophic north Pacific Ocean, Appl. Environ.
596 Microb., 78, 6516-6523, 2012.
597
598 Zeebe, R. E. and Wolf-Gladrow, D. A.: CO2 in seawater: equilibrium, kinetics, isotopes,
599 Elsevier, Amsterdam, 2001.
600
601
602
603
604
605
606
607
608
609
610
611
612
613
614

615 FIGURE HEADINGS

616

617 **Fig. 1.** Mangrove stands sampled along the Saudi coast of the Red Sea. Numbers indicate
618 positions of sampling sites from this study. S1 and S2: King Abdullah University of Science and
619 Technology; S3: Duba; S4 and S5: Al Wahj; S6 and S7: Farasan Banks.

620

621 **Fig. 2.** Change in CO_2 (left panels) and CH_4 (right panels) concentrations over time in triplicated
622 mangrove sediment cores from mangrove stations S3-S7. Shaded areas represent night time and
623 each replicate is coded by different symbols.

624

625 **Fig. 3.** Relationship between day and night fluxes for CO_2 (top panel) and CH_4 (bottom panel) at
626 all mangrove stations.

627

628 **Fig. 4.** Keeling plots for mangrove stations S3-S7, showing the linear regression of the inverse of
629 CO_2 concentration (left panels) and CH_4 concentration (right panels) versus $\delta^{13}C–CO_2$ and $\delta^{13}C–CH_4$. Y-intercepts were used to estimate the isotopic signatures of produced gases.

630

631

632 **Fig. 5.** Relation between the carbon isotopic signature of the produced CO_2 ($\delta^{13}C–CO_2$) and CO_2
633 fluxes (top panel) and carbon isotopic signature of the produced CH_4 ($\delta^{13}C–CH_4$) and the CH_4
634 fluxes (bottom panel) in Red Sea mangroves. Error bars indicate standard error of the mean.

635

636

637

638

639

640

641

642

643

644

Figure 1

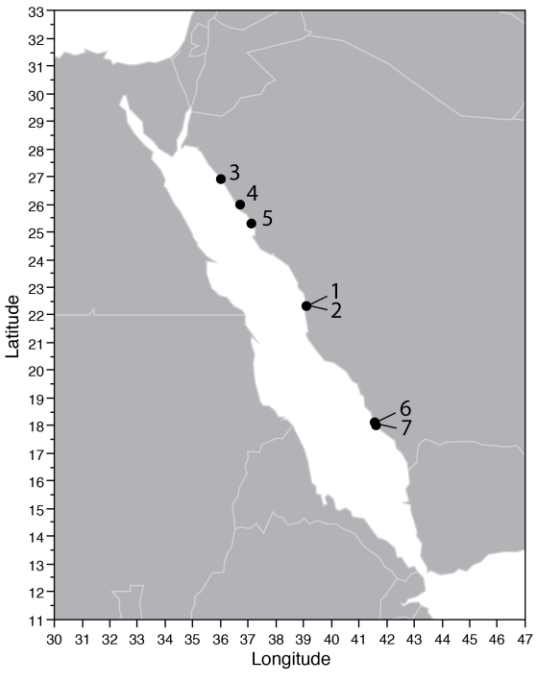

Figure 2

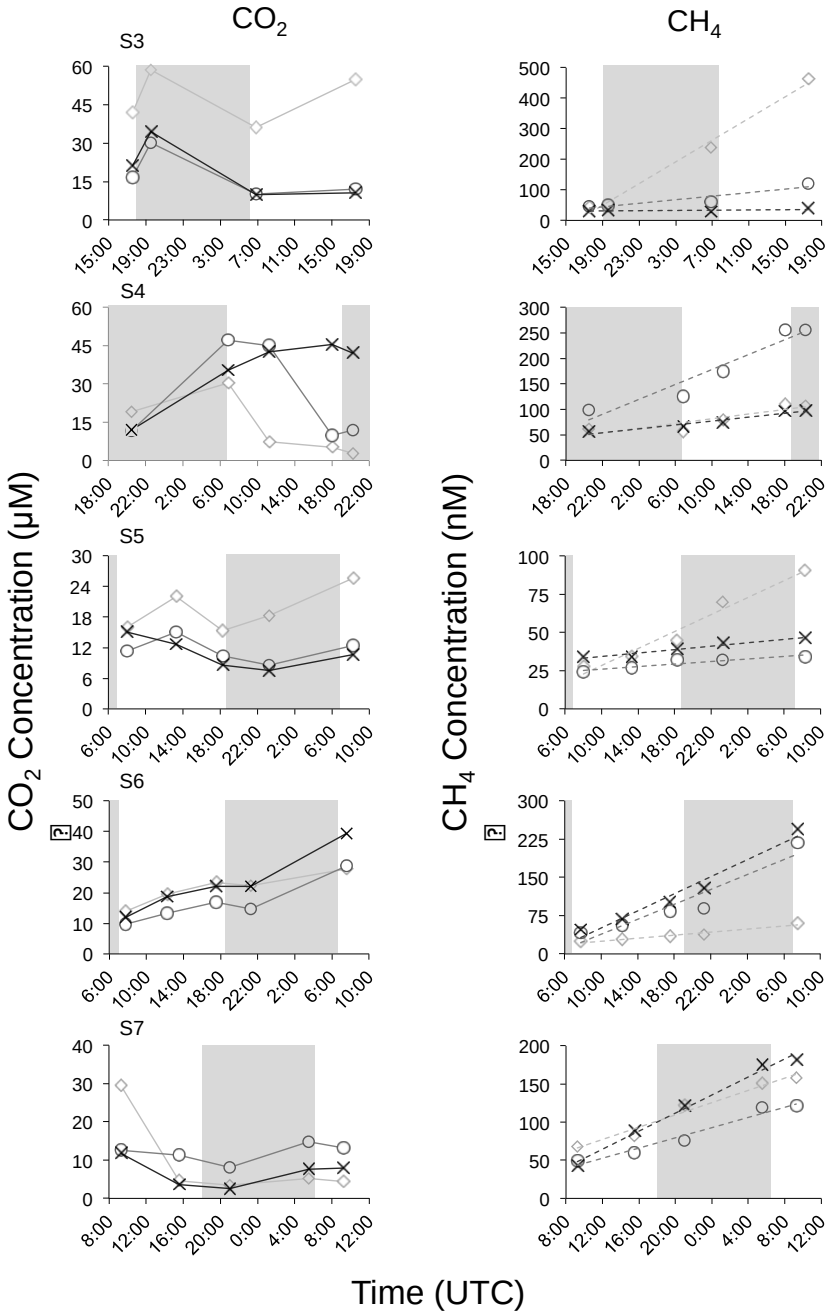
CO2
CH4
S3
S4
S5
S6
S7
CO2 Concentration (µM)
CH4 Concentration (nM)
Time (UTC)

659 **Figure 3**

660

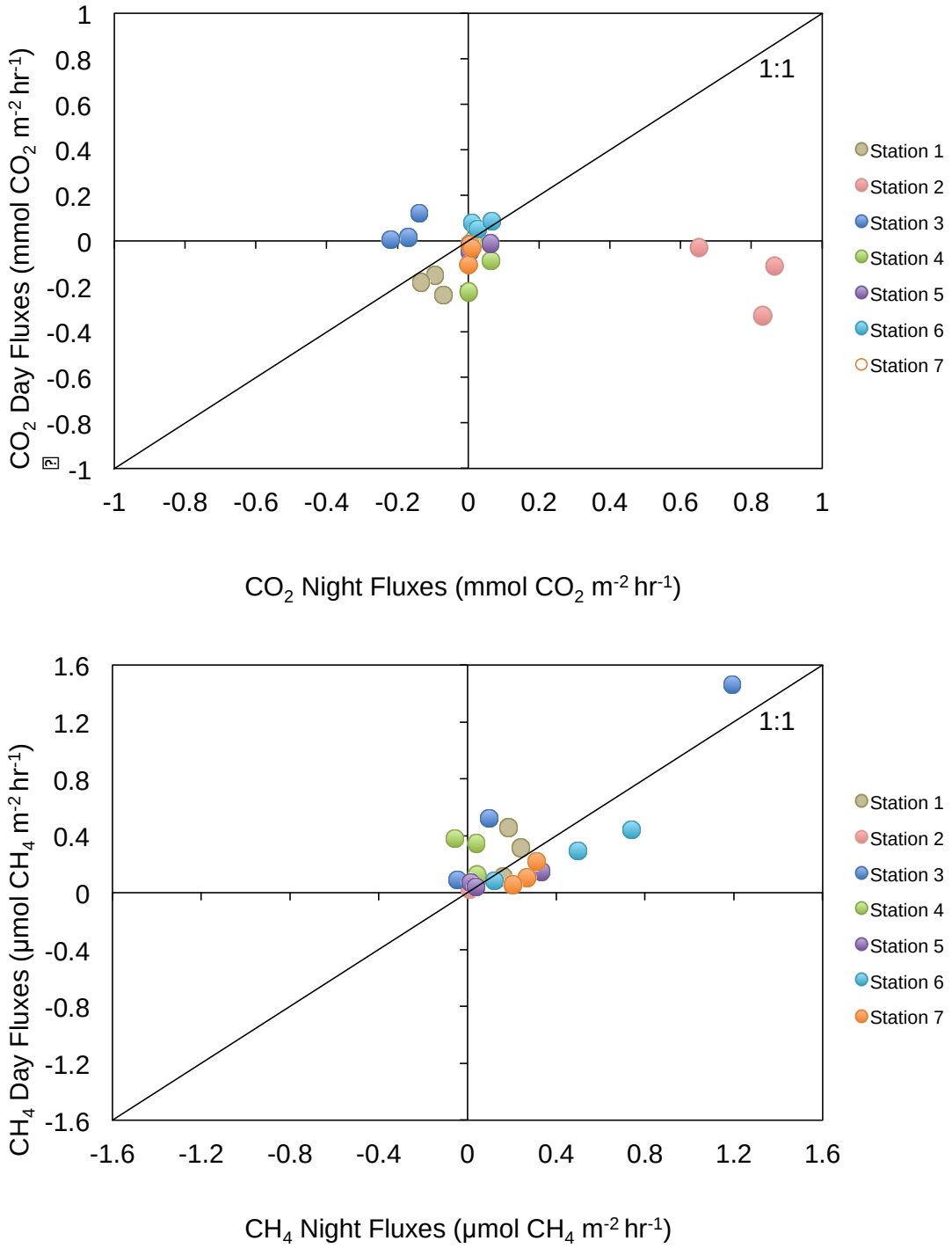

661

662

663 **Figure 4**

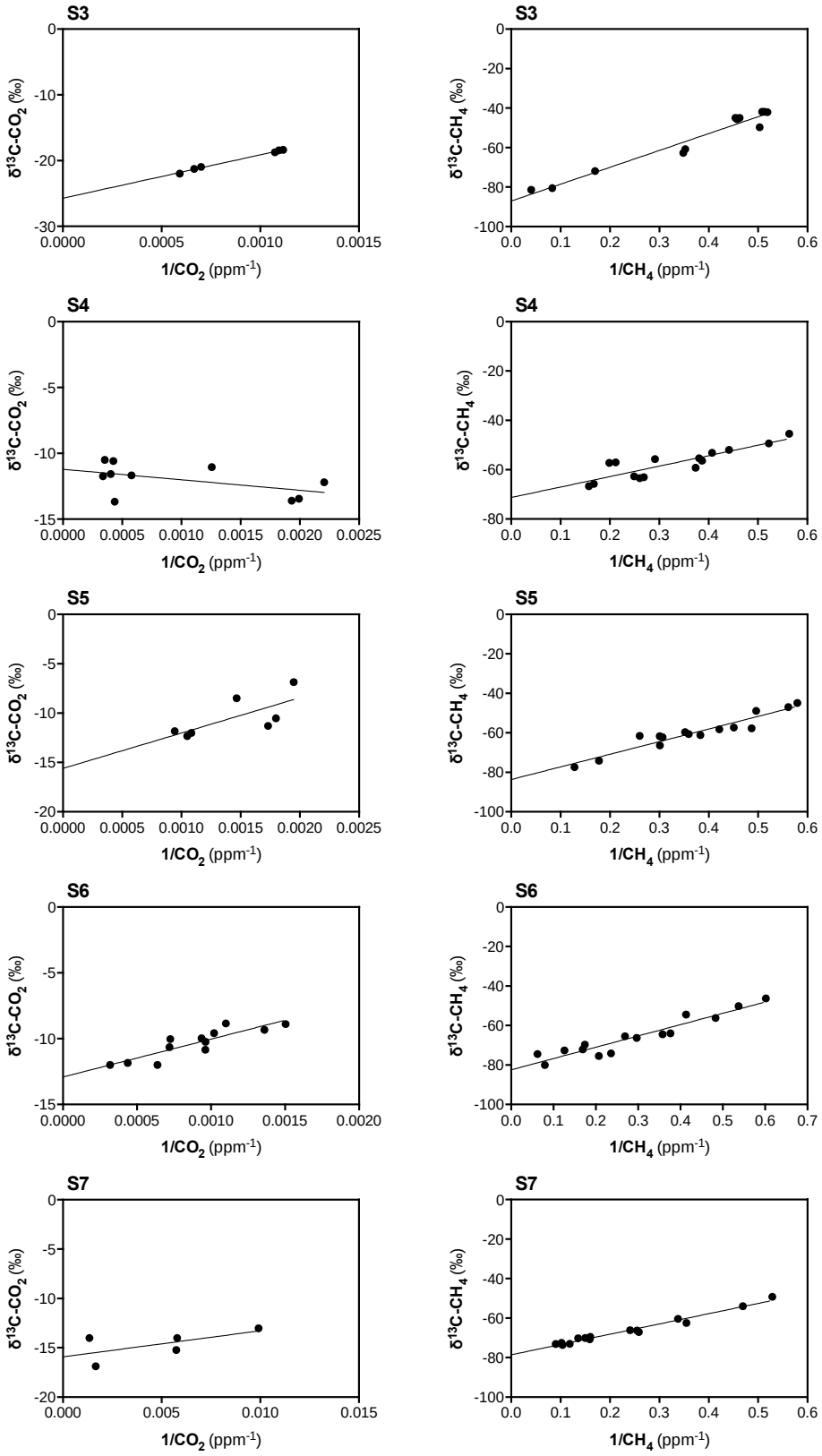

664

Figure 5

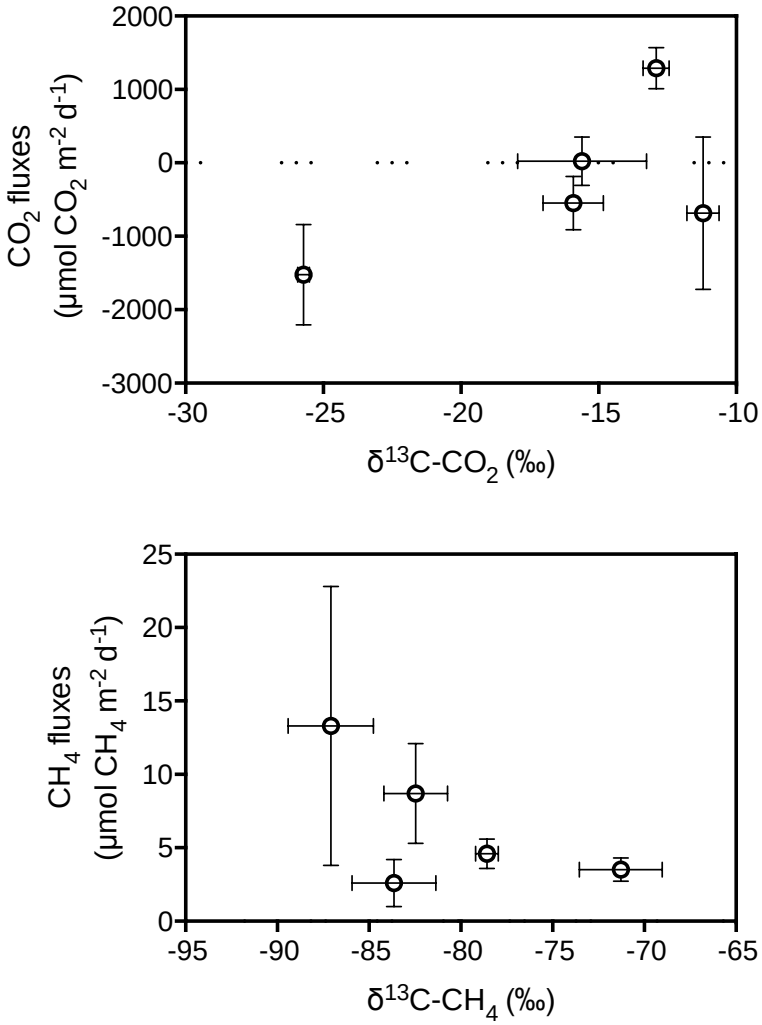
2000
1000
0
-1000
-2000
-3000
-30
-25
-20
-15
-10
CO2 fluxes
(µmol CO2 m-2 d-1)
δ13C-CO2 (‰)
25
20
15
10
5
0
-95
-90
-85
-80
-75
-70
-65
CH4 fluxes
(µmol CH4 m-2 d-1)
δ13C-CH4 (‰)

Table 1. Summary of greenhouse gas fluxes and sediment characteristics from studied mangrove forests. CH_4 fluxes in brackets represent CO_2 equivalents in terms of global warming potential for a time horizon of 100 years (GWP_{100}), taking into account climate-carbon feedback as suggested by the AR5 of IPCC (Myhre et al., 2013). Data represent the mean ± SEM and nd means no data available.

Station	CO_2 Day Flux (µmol CO_2 m^{-2} hr^{-1})	CH_4 Day Flux (µmol CH_4 m^{-2} hr^{-1})	CO_2 Night Flux (µmol CO_2 m^{-2} hr^{-1})	CH_4 Night Flux (µmol CH_4 m^{-2} hr^{-1})	Daily CO_2 Flux (µmol CO_2 m^{-2} d^{-1})	Daily CH_4 Flux (µmol CH_4 m^{-2} d^{-1})	$\delta^{13}C$-CO_2 (‰)	$\delta^{13}C$-CH_4 (‰)	Nitrogen Density (mgN cm^{-3})	C_{org} Density (mgC cm^{-3})	Chl *a* (µg Chl *a*/gr sediment)
1	-188 ± 25	0.30 ± 0.17 [10.2]	-99 ± 18	0.19 ± 0.04 [6.46]	-3452 ± 271	5.9 ± 1.3 [201]	nd	nd	nd	nd	nd
2	-157 ± 89	0.05 ± 0.02 [1.7]	782 ± 66	0.03 ± 0.01 [1.02]	7500 ± 894	0.9 ± 0.25 [31]	nd	nd	nd	nd	nd
3	49 ± 37	0.69 ± 0.4 [23.46]	-176 ± 23	0.42 ± 0.39 [14.28]	-1524 ± 686	13.3 ± 9.5 [452]	-25.7 ± 0.2	-87.1 ± 2.3	1.03 ± 0.05	13.33 ± 1.01	nd
4	-86 ± 79	0.28 ± 0.1 [9.52]	29 ± 19	0.01 ± 0.03 [0.34]	-684 ± 1038	3.5 ± 0.8 [119]	-11.1 ± 0.6	-71.3 ± 2.3	0.80 ± 0.03	8.98 ± 0.86	1.02 ± 0.05
5	-22 ± 11	0.09 ± 0.03 [3.06]	24 ± 20	0.13 ± 0.10 [4.42]	23 ± 331	2.6 ± 1.6 [88]	-15.6 ± 2.3	-83.6 ± 2.3	1.12 ± 0.05	13.34 ± 0.98	1.03 ± 0.04
6	73 ± 10	0.27 ± 0.10 [9.18]	35 ± 17	0.45 ± 0.18 [15.30]	1289 ± 280	8.7 ± 3.4 [296]	-12.9± 0.5	-82.5 ± 1.7	1.51 ± 0.14	10.58 ± 0.82	0.43 ± 0.14
7	-51 ± 28	0.13 ± 0.05 [4.42]	5 ± 3	0.26 ± 0.03 [8.84]	-547 ± 363	4.6 ± 1.0 [156]	-15.9 ± 1.1	-78.6 ± 0.6	3.30 ± 0.55	33.43 ± 6.69	1.86 ± 0.12

Table 2. Comparison of GHG fluxes from global mangrove forests and Red Sea mangroves. Literature values converted from reported form for comparison purposes. Measurements made at the: 1. soil-atmosphere interface, 2. air-sea interface with DIC calculation methods, and 3. air-sea interface with equilibration methods.

			CO_2 (mmol m^{-2} d^{-1})		CH_4 (μmol m^{-2} d^{-1})	
Author	Year	Place	Minimum	Maximum	Minimum	Maximum
Allen et al.[1]	2007	Australia	-	-	4.5	25974
Allen et al.[1]	2011	Australia	-	-	70.3	2348
Alongi et al.[1]	2005	China	17	121	5	66
Chen et al.[1]	2016	China	-16.9	279.2	-2.1	8015.1
Kristensen et al.[1,2]	2008b	Tanzania	28	115	0	87.6
Livesley & Andrusiak[1]	2012	Australia	50	150	50	749
Borges et al.[2]	2003	Papua New Guinea	-	43.6	-	-
Bouillon et al. [2]	2003	India	-	70.2	-	-
Bouillon et al. [2]	2007a	Kenya	3	252	-	-
Bouillon et al. [2]	2007b	Kenya	-	52	-	-
Bouillon et al. [2]	2007c	Tanzania	1	80	-	-
Call et al.[3]	2015	Australia	9.4	629.2	13.1	632.9

Ho et al. [3]	2014	United States	20	118	-	-
Jacotot et al.[3]	2018	New Caledonia	3.12	441.8	4.32	4129.7
Rosentreter et al.[3]	2018a	Australia	58.7	277.6	-	-
Rosentreter et al.[3]	2018b	Australia	-	-	96.5	1049.8
This Study[3]	2017	Red Sea	-3.5	7.5	0.9	13.3